Properties of the K_α X-Ray Transitions in Highly Ionized Chlorine

C. Jiang[a], F. Hu[a,*], Y. Zang[a] and G. Jiang[b]

[a]School of Mathematic and Physical Science, Xuzhou Institute of Technology, Xuzhou 221400, China

[b]Institute of Atomic and Molecular Physics, Sichuan University, Chengdu 610065, China

(Received June 21, 2013; in final form March 19, 2014)

Relativistic configuration interaction calculations with the inclusion of the Breit interaction, quantum electrodynamics and finite nuclear mass corrections have been carried out in the extended optimal level scheme using multi-configuration Dirac–Fock wave functions on the wavelengths, electric dipole transition rates and oscillator strengths of chlorine. Through the use of the active space method, the calculated values are compared with the other available data on He-like and Be-like chlorine and are found to be in very good agreement with them. In this paper we give accurate transition properties from Cl(VIII) through Cl(XVI). These data provide reference value for level lifetime, charge state distribution and average charge of chlorine plasma.

DOI: 10.12693/APhysPolA.126.694

PACS: 31.15.V−, 31.30.jc

1. Introduction

Chlorine is a trace element in astrophysical and atmospheric plasmas, and can occur in some laboratory plasmas and industrial processes such as polysilicon etching in Cl plasmas. Both from the plasma modeling point of view and from spectroscopic diagnostics it can be important to know the radiative properties of atomic and ionic Cl.

In 2002, Berrington and Nakazaki [1] reported a comprehensive study of radiative data for neutral chlorine and its ions. They clearly demonstrated the importance and need for further studies on these ions as there are either very few or virtually no data available for ions of Cl. The *R*-matrix approach employed by Berrington and Nakazaki is perhaps the only reported detailed study on ions of Cl. Later, new theoretical and experimental results for Cl(I) have been reported by Deb et al. [2], Singh et al. [3], Oliver and Hibbert [4, 5], and Bridges and Wiese [6]. To supply more data for Cl ions, Tayal presented the oscillator strengths for Cl(II) [7]. Transition probabilities for Cl(III) were done by Schectman et al. and Mossah [8, 9]. Energy levels for Cl(IV) were presented by Abou el-Maaref et al. [10]. Choudhury et al. calculated transitions for Cl(V) [11]. Energy levels for Cl(VI) were reported by Neerja et al. [12]. Theoretical lifetimes and wavelengths for Cl(X) configurations were from Bogdanovich et al. [13, 14]. Very recently, energy levels and radiative rates for Cl(XVI) were displayed by Aggarwal and Keenan [15].

Although accurate transition data in highly ionized chlorine is important in a variety of scientific applications, systematic calculations on the K_α X-ray spectra of chlorine are still fragmentary, especially from B-like to Ne-like. The features of chlorine K-lines have been investigated to develop X-ray probes for Compton scattering on warm dense plasmas [16]. So it is essential to study the properties of these lines in detail, so our investigation is motivated by the need for accurate transition data in a variety of scientific applications.

In this paper, we display and discuss the results of our calculations of transition wavelengths, absorption oscillator strengths, transition probability and line strengths of chlorine atoms from Cl(VIII) through Cl(XVI) in the framework of relativistic configuration interaction formalism by using MCDF wave functions. The configuration interaction calculations include the Breit interaction, quantum electrodynamics (QED) and nuclear mass corrections. A substantial amount of relaxations of atomic orbitals have been included in this work. In this paper, the GRASPVU package (a general purpose relativistic atomic structure package) was used. It is a modified and parallel version of the Grasp92 package [17–20].

2. Method of calculation

The extended optimal level (EOL) version of the multi-configuration Dirac–Fock (MCDF) method is used to calculate the transitions. The theoretical basis of our present computational approach has been widely discussed elsewhere [17–21]. Hence we only repeat the essential features here.

The GRASPVU package is based on MCDF method. In MCDF method the atom is represented by atomic state functions (ASF), which are a linear combination of configuration state functions (CSF)

$$\Psi(\gamma J) = \sum_i c_i \Phi_i(\alpha_i J), \tag{1}$$

where the CSF $\Phi(\alpha J)$ are antisymmetrized linear combinations of relativistic orbital products of the form

$$\phi(\boldsymbol{r}) = \frac{1}{\boldsymbol{r}} \begin{pmatrix} P_{n\kappa}(\boldsymbol{r})\chi_{\kappa m}(\boldsymbol{r}) \\ \mathrm{i}Q_{n\kappa}(\boldsymbol{r})\chi_{-\kappa m}(\boldsymbol{r}) \end{pmatrix}. \tag{2}$$

*corresponding author; e-mail: hufengscu@139.com

Here κ is the relativistic angular momentum, $P_{n\kappa}(\boldsymbol{r})$ and $Q_{n\kappa}(\boldsymbol{r})$ are the large and small component radial wave functions and $\chi_{\kappa m}(\boldsymbol{r})$ is the spinor spherical harmonic in the lsj coupling scheme. The CSF are constructed from one-electron orbitals, according to the well-known rules of symmetry. The goal is a systematic approach, where all important contributions are included. This allows for monitoring the convergence of different properties and plausible estimates of uncertainties. The foundation of the method is an active set of orbitals, which is used to generate all possible CSF. The size, and thereby the accuracy, of a certain approach is therefore defined by the size of the active set of orbitals. It is thus straightforward to define a systematic approach, by just increasing the orbital set in a systematic fashion.

The Dirac–Coulomb Hamiltonian can be written as

$$\hat{H}^{\mathrm{DC}} = \sum_{i}^{N} \hat{H}_{\mathrm{D}}(i) + \sum_{i=1}^{N-1} \sum_{j=i+1}^{N} |\hat{r_i} - \hat{r_j}|^{-1} . \qquad (3)$$

All the dominant interactions in an N-electron atom or ion are included in the Dirac–Coulomb Hamiltonian. In Eq. (3), the first term is the one-body contribution for an electron due to the kinetic energy and interaction with the nucleus. The two-body Coulomb interaction between the electrons comprises the second term. Higher order modifications to Eq. (3) due to the transverse electromagnetic interaction and the radiative corrections are treated via perturbation theory.

This work was performed using an expansion of configuration interaction based on MCDF method. To build a CSF expansion, the restrictive active space methods were used. The idea of the active space methods is to consider only electrons from the active set and to excite them from the occupied orbitals to unoccupied ones. The orbital was increased systematically in order to monitor the convergence of the calculation. Since the orbitals with the same principal quantum number n often have similar energies, the active set is usually enlarged in steps of orbital layers. It is convenient to refer to the $\{1s, 2s, 2p, 3s, 3p, 3d\}$ set of orbitals as the $n = 3$ orbital layer, $\{1s, 2s, 2p, \ldots 4s, 4p, 4d, 4f\}$ as $n = 4$, etc. Larger orbital sets can result in a considerable increase of computational time required for the problem, and appropriate restrictions may be necessary. Based on above calculation method, we considered the active space consisting of all the orbitals in the set with principal quantum number $n = 1{-}7$ and $l = s$ to g were included with $n = 8$. All electrons were treated as reference configurations throughout the present calculations.

Succeeding the generation of the CSF sets, we perform angular integrations for the matrix elements of the many-electron Dirac–Coulomb Hamiltonian. To generate initial estimates for radial orbitals, we used a Thomas–Fermi potential. The optimizations were carried out layer by layer to obtain the orbitals requested in next CI calculation. In this scheme, first we optimized the orbitals with $n \leq 3$ in the reference CSFs. Then we optimized the orbitals for $n = 4$ layer and kept the $n \leq 3$ orbitals fixed. With this scheme we optimized $n = 5$. The optimization is on the $(2J + 1)$ weighted average of all fine structure levels belonging to an LS term and the driven to convergence with the self-consistency criteria set to 10^{-8}.

In all our calculations we used the method of block structuring of the Hamiltonian. The advantage of this block mode is that it results in a considerable reduction in the memory requirement when dealing with atomic states of different total angular momentum and parity. Each block corresponds to a given J and parity and hence it is possible to specify the required eigenstates that are to be obtained for the specific block rather than the whole Hamiltonian matrix. We finally converted the block mode into non-block mode while calculating the transition rates.

Once the RCI energies and wave functions were obtained, the mixing coefficient was transformed from the block format to non-block format. Then the initial and final orbital sets were transformed to become bi--orthonormal and the oscillator strengths, line strengths, transition probabilities were calculated.

3. Results and discussion

The EOL scheme used in this work includes several levels in the energy functional that takes into account the weights for the levels under consideration. Using jj coupled states as basis states, the Dirac–Fock calculations were first performed for the reference configurations $1s2s^l2p^m$ and $1s^22s^l2p^{m-1}$. Then the correlation effects were included by continuing the calculations for a series of expansions generated mainly by single and double (SD) electron replacements from the configuration of interest (reference configuration) to an active set of orbitals with the same LS symmetry. The virtual set was varied in a systematic way by increasing the principal quantum number n by one without imposing restrictions on the orbital quantum number. Earlier calculations [22] indicate that the set that could be handled without any difficulty was up to $n = 4$. Also, for configurations with more than four electrons, the number of CSFs generated was very large for double excitation and we could not carry out our RCI calculations due to storage limitations. However, to illustrate the convergence of energy eigenvalues for different active sets, we carried out MCDF calculations on the $1s2p$ and $1s^2$ configurations of chlorine by considering all the virtual shells up to $n = 8$. When $n = 8$, the number of CSFs generated for single excitation was 122, while for double excitation the number up to 1424.

Single and double excitations for some specific states of initial and final configurations were given in Table I. Our calculations showed that the difference in the energy values obtained with single and double excitations were negligible, and we can also get it from Ref. [23]. In that paper, the author reported that the number of CSFs for double excitation increases many-fold with the increase in the size of the active set, which gives rise to software problems. To keep the CSFs at a manageable level and consider the size of the numerical calculations involved in this work we restricted to single excitation only. Also to

keep CSFs, the principal number n was limited in whole calculation ($n \leq 6$).

TABLE I

Energies of the $1s^1 2p^1\ ^1P_1$ and $1s^2\ ^1S_0$ terms of chlorine in atomic unit (a.u.) for single and double excitation of the active sets of orbitals.

Term	Active set	Single	Double
$1s^1 2p^1\ ^1P_1$	$n = 2$	−279.415	−279.419
	$n = 3$	−279.416	−279.421
	$n = 4$	−279.416	−279.421
	$n = 5$	−279.417	−279.423
	$n = 6$	−279.417	−279.423
	$n = 7$	−279.417	−279.423
	$n = 8$	−279.418	−279.424
$1s^2\ ^1S_0$	$n = 2$	−176.943	−176.942
	$n = 3$	−176.944	−176.945
	$n = 4$	−176.944	−176.945
	$n = 5$	−176.946	−176.949
	$n = 6$	−176.946	−176.949
	$n = 7$	−176.946	−176.951
	$n = 8$	−176.947	−176.951

TABLE II

Selected line strengths obtained from MCDF and RCI model. Percent differences were computed according to the formula $[L_{\rm v} - L_{\rm l}] \times 100/\max\{L_{\rm v}, L_{\rm l}\}$.

Transitions	n	$L_{\rm v}$	$L_{\rm l}$	Difference [%]
$^3P_1 - {}^1S_0$	2	0.012453	0.012339	0.92
	3	0.012441	0.012373	0.55
	4	0.012435	0.012398	0.29
	5	0.012407	0.012380	0.21
	6	0.012381	0.012354	0.21
$^1P_1 - {}^1S_0$	2	0.112853	0.112307	0.48
	3	0.111748	0.111516	0.20
	4	0.111348	0.111274	0.06
	5	0.111025	0.110966	0.05
	6	0.111016	0.110955	0.05

In order to validate the present model and make sure that the calculations based on the present model are accurate, a comparison of transition line strengths of He-like chlorine ions is given in Table II. The transition rates are, in general, calculated in length and velocity gauge. We monitored the length and velocity forms of the MCDF and RCI line strengths for orbital sets of increasing size, denoted by n. In Table II, we present two selected transitions. As can be seen from this, the agreement of the two gauges is very good and the near equal values of the length and velocity of the transitions give an additional check on the accuracy of our results. The agreement of the two gauges improves with increasing n. At the same time, we can find that the length forms for transitions are usually considered to be more stable because they probe the wave function in a similar region as does the optimization procedure on the total energy of the atoms or ions [24–26]. For this reason, we use length gauge in our present work.

TABLE III

Comparisons between our calculated values and the experimental values for He-like and Li-like chlorine.

Transition (E1)	Wavelength [Å]	Transition probability [s^{-1}]	Oscillator strength
$1s2p - 1s^2$			
$^3P_1 - {}^1S_0$	4.4681[a]	1.0524(12)[a]	9.4497(−3)[a]
	4.4717[b]	1.0193(12)[b]	9.1666(−4)[b]
	4.4677[c]		
	4.4669[d]		
$^1P_1 - {}^1S_0$	4.4445[a]	8.4674(13)[a]	7.5228(−1)[a]
	4.4473[b]	8.6890(13)[b]	7.7291(−1)[b]
	4.4442[c]		
	4.4438[d]		
$1s2s2p - 1s^2 2s$			
$^4P_{1/2} - {}^2S_{1/2}$	4.5246[a]	9.5493(10)[a]	5.8614(−4)[a]
	4.5372[b]	1.1101(11)[b]	6.8522(−4)[b]
$^4P_{3/2} - {}^2S_{1/2}$	4.5235[a]	2.6137(11)[a]	3.2073(−3)[a]
	4.5361[b]	2.8446(11)[b]	3.5098(−3)[b]
$(^3S)^2 P_{3/2} - {}^2S_{1/2}$	4.4673[a]	4.2073(12)[a]	5.0352(−2)[a]
	4.4795[b]	2.4135(13)[b]	1.4520(−1)[b]
	4.4666[d]		
	4.4669[e]		
$(^3S)^2 P_{1/2} - {}^2S_{1/2}$	4.4681[a]	1.3501(13)[a]	8.0818(−2)[a]
	4.4798[b]	1.5892(13)[b]	1.9126(−1)[b]
	4.4675[d]		
	4.4649[e]		
$(^1S)^2 P_{3/2} - {}^2S_{1/2}$	4.4838[a]	7.7278(13)[a]	9.3169(−1)[a]
	4.5017[b]	6.7059(13)[b]	8.1491(−1)[b]
	4.4829[d]		
	4.4837[e]		
$(^1S)^2 P_{1/2} - {}^2S_{1/2}$	4.4859[a]	6.8145(13)[a]	4.1117(−1)[a]
	4.5050[b]	5.8988(13)[b]	3.5895(−1)[b]
	4.4850[d]		
	4.4837[e]		

[a] present GRASPVU calculations;
[b] present GRASP^2 calculations;
[c] Ref. [25]; [d] Ref. [26]; [e] Ref. [27]

In order to check the reliability of our calculation, our calculated values for transitions from He-like and Li-like chlorine is compared with the states calculated using GRASP^2 [27] with the other theoretical and experimental data [28, 29]. The present wavelengths are in good agreement with the experimental values. However, a more detailed comparison of the calculated and experimental wavelengths for these transitions (Table III) indicates that the transition wavelengths given by our GRASPVU calculations are in better agreement with the experimental wavelengths than our GRASP^2 results. The maximum difference between the results of experimental and our GRASPVU transition wavelengths is 0.071%, but the maximum difference for our GRASP^2 and the experimental is 0.401%.

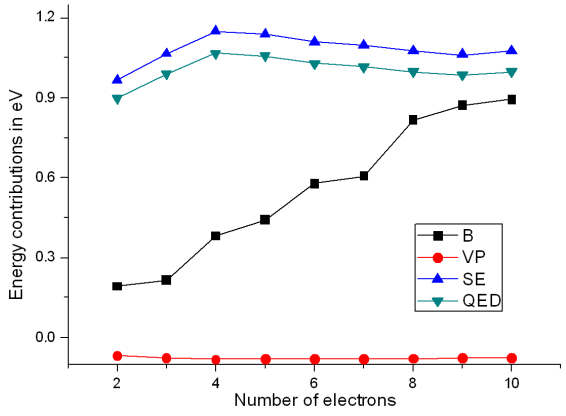

Fig. 1. Contributions from Breit interaction (B), self--energy (SE), vacuum polarization (VP) to the final weighted sum of configurations from Cl(VIII) through Cl(XVI).

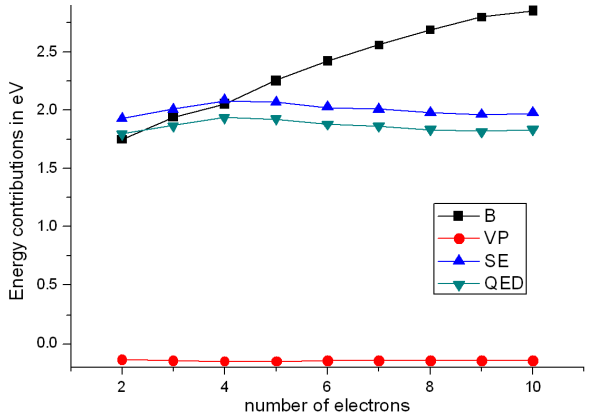

Fig. 2. Contributions from Breit interaction (B), self--energy (SE), vacuum polarization (VP) to the initial weighted sum of configurations from Cl(VIII) through Cl(XVI).

For the method of GRASP[2], the computations were done with the extended average level (EAL) option. Rather than optimizing one orbital at a time as in GRASPVU, all the orbitals which are included are optimized simultaneously on the average energy of all the configurations according to some weighting scheme — in our case we simply used the option which weights each level equally. Zero-order Coulomb eigenvectors and energy levels are calculated first by the code. The full transverse Breit interaction is added to the Hamiltonian and a further diagonalization in the configurations basis yields Breit-corrected eigenvectors and energy levels.

Lastly, QED energy corrections were estimated and added. There are two major components in the QED correction. The dominant one is the self-energy. The leading term of a less-dominant QED correction is the vacuum polarization.

The contributions from Breit interaction, and QED to the weighted sum of configuration-average energy levels of K_α initial and final configurations from Cl(VIII) to

TABLE IV

Our calculations on the K_α X-ray wavelength, transition probability (A), absorption oscillator strengths (gf) in length gauge and the ratios of velocity to length rates ($A_\mathrm{v}/A_\mathrm{l}$) from Cl(VIII) through Cl(XVI).

Transition K_α X-ray	Wavelength [Å]	Transition probability [s^{-1}]	Oscillator strength	$A_\mathrm{v}/A_\mathrm{l}$
$1s2p-1s^2$				
$^3P_1-{}^1S_0$	4.4681(0)	1.0524(12)	9.4497(−3)	1.004
$^1P_1-{}^1S_0$	4.4445(0)	8.4674(13)	7.5228(−1)	1.001
$1s2s2p-1s^22s$				
$^4P_{1/2}-{}^2S_{1/2}$	4.5246(0)	9.5493(10)	5.8614(−4)	1.003
$^4P_{3/2}-{}^2S_{1/2}$	4.5235(0)	2.6137(11)	3.2073(−3)	1.001
$(^3S)^2P_{3/2}-{}^2S_{1/2}$	4.4673(0)	4.2073(12)	5.0352(−2)	0.977
$(^3S)^2P_{1/2}-{}^2S_{1/2}$	4.4681(0)	1.3501(13)	8.0818(−2)	0.992
$(^1S)^2P_{3/2}-{}^2S_{1/2}$	4.4838(0)	7.7278(13)	9.3169(−1)	1.002
$(^1S)^2P_{1/2}-{}^2S_{1/2}$	4.4859(0)	6.8145(13)	4.1117(−1)	1.003
$1s2s^22p-1s^22s^2$				
$^3P_1-{}^1S_0$	4.5442(0)	8.9751(11)	8.3353(−3)	0.989
$^1P_1-{}^1S_0$	4.5207(0)	7.9214(13)	7.2808(−1)	0.970
$1s2s^22p^2-1s^22s^22p$				
$^4P_{1/2}-{}^2P_{1/2}$	4.5948(0)	2.7362(11)	1.7320(−3)	0.957
$^2P_{3/2}-{}^2P_{1/2}$	4.5597(0)	7.3134(12)	9.1180(−2)	0.957
$^2P_{1/2}-{}^2P_{1/2}$	4.5636(0)	8.1330(13)	5.0786(−1)	0.958
$^4P_{3/2}-{}^2P_{1/2}$	4.5930(0)	1.2329(09)	1.5596(−5)	0.971
$^2D_{3/2}-{}^2P_{1/2}$	4.5675(0)	4.2382(13)	5.3020(−1)	0.960
$^2S_{1/2}-{}^2P_{1/2}$	4.5452(0)	5.6884(12)	3.5235(−2)	0.949
$^4P_{1/2}-{}^2P_{3/2}$	4.5985(0)	3.3626(10)	2.1320(−4)	0.947
$^2P_{3/2}-{}^2P_{3/2}$	4.5634(0)	9.9407(13)	1.2414(00)	0.958
$^4P_{5/2}-{}^2P_{3/2}$	4.5948(0)	3.3481(11)	6.3581(−3)	0.962
$^2P_{1/2}-{}^2P_{3/2}$	4.5673(0)	2.9499(13)	1.8450(−1)	0.959
$^4P_{3/2}-{}^2P_{3/2}$	4.5967(0)	1.9461(11)	2.4659(−3)	0.961
$^2D_{5/2}-{}^2P_{3/2}$	4.5712(0)	2.0089(10)	2.5173(−4)	0.923
$^2D_{3/2}-{}^2P_{3/2}$	4.5712(0)	3.7062(13)	6.9661(−1)	0.961
$^2S_{1/2}-{}^2P_{3/2}$	4.5489(0)	3.2872(13)	2.0395(−1)	0.952
$1s2s^22p^3-1s^22s^22p^2$				
$^3S_1-{}^3P_0$	4.6008(0)	1.7952(13)	1.7090(−1)	0.953
$^3D_1-{}^3P_0$	4.6085(0)	2.4811(13)	2.3699(−1)	0.956
$^3P_1-{}^3P_0$	4.5936(0)	3.6178(12)	3.4334(−2)	0.948
$^1P_1-{}^3P_0$	4.5744(0)	6.1382(08)	5.7767(−6)	0.854
$^5S_2-{}^3P_1$	4.6413(0)	5.7079(10)	9.2165(−4)	0.953
$^3S_1-{}^3P_1$	4.6023(0)	5.6907(13)	5.4210(−1)	0.954
$^1D_2-{}^3P_1$	4.5897(0)	6.8276(11)	1.0781(−2)	0.950
$^3D_1-{}^3P_1$	4.6100(0)	9.4021(12)	8.9866(−2)	0.958
$^3P_0-{}^3P_1$	4.5952(0)	3.4825(13)	1.1024(−1)	0.951
$^3D_2-{}^3P_1$	4.6100(0)	3.0622(13)	4.8781(−1)	0.956
$^3P_1-{}^3P_1$	4.5951(0)	3.2031(12)	3.0417(−2)	0.950
$^3P_2-{}^3P_1$	4.5959(0)	3.4809(12)	5.5112(−2)	0.949
$^1P_1-{}^3P_1$	4.5759(0)	6.0183(10)	5.6675(−3)	0.952
$^5S_2-{}^3P_2$	4.6433(0)	9.2501(10)	1.4949(−3)	0.949
$^3S_1-{}^3P_2$	4.6043(0)	5.8668(13)	5.5936(−1)	0.954
$^1D_2-{}^3P_2$	4.5917(0)	2.8056(11)	4.4340(−3)	0.942
$^3D_3-{}^3P_2$	4.6120(0)	8.7172(11)	8.3393(−3)	0.958
$^3D_1-{}^3P_2$	4.6123(0)	3.4275(13)	7.6518(−1)	0.957
$^3D_2-{}^3P_2$	4.6120(0)	3.8811(12)	6.1881(−2)	0.959
$^3P_1-{}^3P_2$	4.5971(0)	3.2860(13)	3.1232(−1)	0.952
$^3P_2-{}^3P_2$	4.5979(0)	3.1688(13)	5.0215(−1)	0.952
$^1P_1-{}^3P_2$	4.5779(0)	3.2951(08)	3.1057(−6)	0.793
$^5S_2-{}^1D_2$	4.6570(0)	7.9519(08)	1.2927(−5)	0.958
$^3S_1-{}^1D_2$	4.6177(0)	1.5248(11)	1.4623(−3)	0.959
$^1D_2-{}^1D_2$	4.6051(0)	9.5890(13)	1.5242(00)	0.955
$^3D_3-{}^1D_2$	4.6255(0)	2.4104(11)	2.3194(−3)	0.946
$^3D_1-{}^1D_2$	4.6258(0)	5.7340(11)	1.2876(−2)	0.956
$^3D_2-{}^1D_2$	4.6255(0)	3.2938(11)	5.2824(−3)	0.958
$^3P_1-{}^1D_2$	4.6105(0)	1.1624(11)	1.1113(−3)	0.952
$^3P_2-{}^1D_2$	4.6113(0)	7.1434(12)	1.1386(−1)	0.956
$^1P_1-{}^1D_2$	4.5912(0)	5.8262(13)	5.5233(−1)	0.949
$^3S_1-{}^1S_0$	4.6394(0)	2.2616(10)	2.1893(−4)	0.976
$^3D_1-{}^1S_0$	4.6472(0)	8.7150(09)	8.4648(−5)	0.978
$^3P_1-{}^1S_0$	4.6321(0)	2.7857(11)	2.6881(−3)	0.954
$^1P_1-{}^1S_0$	4.6126(0)	4.6064(13)	4.4077(−1)	0.958

TABLE IV (cont.)

Transition K_α X-ray	Wavelength [Å]	Transition probability [s^{-1}]	Oscillator strength	A_v/A_l
$1s2s^22p^4-1s^22s^22p^3$				
$^4P_{5/2}-{}^4S_{3/2}$	4.6451(0)	3.2528(13)	6.3132(−1)	0.947
$^4P_{3/2}-{}^4S_{3/2}$	4.6424(0)	3.2510(13)	4.2016(−1)	0.947
$^4P_{1/2}-{}^4S_{3/2}$	4.6141(0)	7.1076(09)	4.5371(−5)	0.959
$^2D_{3/2}-{}^4S_{3/2}$	4.6206(0)	2.2449(07)	2.8741(−7)	0.711
$^2D_{5/2}-{}^4S_{3/2}$	4.6205(0)	3.5044(10)	6.7296(−4)	0.938
$^2P_{1/2}-{}^4S_{3/2}$	4.6412(0)	3.2489(13)	2.0983(−1)	0.947
$^2P_{3/2}-{}^4S_{3/2}$	4.6157(0)	5.6582(10)	7.2288(−4)	0.949
$^2S_{1/2}-{}^4S_{3/2}$	4.5992(0)	1.2744(08)	8.0824(−7)	0.946
$^4P_{5/2}-{}^2D_{3/2}$	4.6658(0)	3.8487(10)	7.5364(−4)	0.947
$^4P_{3/2}-{}^2D_{3/2}$	4.6630(0)	1.1169(11)	1.4564(−3)	0.949
$^4P_{1/2}-{}^2D_{3/2}$	4.6345(0)	6.8839(13)	4.4332(−1)	0.944
$^2D_{3/2}-{}^2D_{3/2}$	4.6411(0)	6.0121(13)	7.7655(−1)	0.947
$^2D_{5/2}-{}^2D_{3/2}$	4.6409(0)	1.2285(12)	2.3800(−2)	0.943
$^2P_{1/2}-{}^2D_{3/2}$	4.6619(0)	2.4751(10)	1.6129(−4)	0.947
$^2P_{3/2}-{}^2D_{3/2}$	4.6362(0)	1.1408(12)	1.4704(−2)	0.946
$^2S_{1/2}-{}^2D_{3/2}$	4.6194(0)	1.9467(10)	1.2455(−4)	0.937
$^4P_{5/2}-{}^2D_{5/2}$	4.6661(0)	2.6832(11)	5.2549(−3)	0.949
$^4P_{3/2}-{}^2D_{5/2}$	4.6633(0)	4.2782(10)	5.5789(−4)	0.944
$^2D_{3/2}-{}^2D_{5/2}$	4.6413(0)	1.2804(12)	1.6540(−2)	0.943
$^2D_{5/2}-{}^2D_{5/2}$	4.6412(0)	4.5339(13)	8.7847(−1)	0.947
$^2P_{3/2}-{}^2D_{5/2}$	4.6364(0)	7.6942(13)	9.9182(−1)	0.945
$^4P_{3/2}-{}^2P_{1/2}$	4.6775(0)	4.0611(09)	5.3282(−5)	0.962
$^4P_{1/2}-{}^2P_{1/2}$	4.6488(0)	4.0183(13)	2.6038(−1)	0.950
$^2D_{3/2}-{}^2P_{1/2}$	4.6554(0)	5.5463(12)	7.2081(−2)	0.953
$^2P_{1/2}-{}^2P_{1/2}$	4.6764(0)	7.1035(10)	4.6576(−4)	0.947
$^2P_{3/2}-{}^2P_{1/2}$	4.6505(0)	1.6056(13)	2.0823(−1)	0.979
$^2S_{1/2}-{}^2P_{1/2}$	4.6336(0)	1.4125(13)	9.0931(−2)	0.942
$^4P_{5/2}-{}^2P_{3/2}$	4.6808(0)	1.2298(09)	2.4238(−5)	0.902
$^4P_{3/2}-{}^2P_{3/2}$	4.6780(0)	1.7775(10)	2.3326(−4)	0.940
$^4P_{1/2}-{}^2P_{3/2}$	4.6494(0)	1.9803(13)	1.2835(−1)	0.949
$^2D_{3/2}-{}^2P_{3/2}$	4.6559(0)	6.9056(12)	8.9769(−2)	0.953
$^2D_{5/2}-{}^2P_{3/2}$	4.6558(0)	1.8397(13)	3.5871(−1)	0.952
$^2P_{1/2}-{}^2P_{3/2}$	4.6769(0)	4.8939(10)	3.2095(−4)	0.948
$^2P_{3/2}-{}^2P_{3/2}$	4.6510(0)	2.7064(13)	3.5106(−1)	0.950
$^2S_{1/2}-{}^2P_{3/2}$	4.6342(0)	5.2341(13)	3.3702(−1)	0.944
$1s2s^22p^5-1s^22s^22p^4$				
$^3P_2-{}^3P_2$	4.6757(0)	4.4766(13)	7.3362(−1)	0.944
$^3P_1-{}^3P_2$	4.6732(0)	2.5428(13)	2.4975(−1)	0.944
$^1P_1-{}^3P_2$	4.6566(0)	1.9639(11)	1.9153(−3)	0.939
$^3P_1-{}^3P_0$	4.6762(0)	2.0147(13)	1.9814(−1)	0.944
$^1P_1-{}^3P_0$	4.6597(0)	4.5610(09)	4.4539(−5)	0.923
$^3P_2-{}^3P_1$	4.6781(0)	1.5183(13)	2.4906(−1)	0.945
$^3P_1-{}^3P_1$	4.6755(0)	1.4924(13)	1.4672(−1)	0.944
$^1P_1-{}^3P_1$	4.6589(0)	1.4860(11)	1.4506(−3)	0.940
$^3P_0-{}^3P_1$	4.6736(0)	6.0071(13)	1.9670(−1)	0.944
$^3P_2-{}^1D_2$	4.6906(0)	4.4480(11)	7.3357(−3)	0.948
$^3P_1-{}^1D_2$	4.6881(0)	3.0327(13)	2.9977(−3)	0.947
$^1P_1-{}^1D_2$	4.6714 (0)	9.9569(13)	9.7719(−1)	0.943
$^3P_1-{}^1S_0$	4.7088(0)	1.6750(09)	1.6703(−5)	0.987
$^1P_1-{}^1S_0$	4.6920(0)	2.0045(13)	1.9846(−1)	0.951
$1s2s^22p^6-1s^22s^22p^5$				
$^2S_{1/2}-{}^2P_{3/2}$	4.7047(0)	5.5632(13)	3.6920(−1)	0.937
$^2S_{1/2}-{}^2P_{1/2}$	4.7076(0)	2.8233(13)	1.8760(−1)	0.939
$1s2s^22p^63s-1s^22s^22p^53s$				
$^3S_1-{}^3P_2$	4.7087(0)	4.6021(13)	4.5891(−1)	0.934
$^3S_1-{}^3P_1$	4.7099(0)	2.1733(13)	2.1682(−1)	0.935
$^1S_0-{}^3P_1$	4.7062(0)	1.7901(13)	5.9438(−2)	0.933
$^3S_1-{}^3P_0$	4.7116(0)	9.3440(12)	9.3289(−2)	0.936
$^3S_1-{}^1P_1$	4.7132(0)	6.1594(12)	6.1536(−2)	0.936
$^1S_0-{}^1P_1$	4.7094(0)	6.5373(13)	2.1736(−1)	0.935

Cl(XVI) are displayed in Figs. 1 and 2, respectively. It can be seen from the figures that the Breit interaction and self-energy are dominant and self-energy occupies a large weight in QED corrections. With increasing number of electrons, the Breit energy increases as is evident from the figures, whereas self-energy changes slightly and vacuum polarization is nearly constant. From the two figures, we can predict that the Breit interaction will increase with the decrease in ionization, especially in neutral atoms. This can be explained as follows: compared with highly ionized ions, in lowly ionized atoms and neutral atoms the nuclear charge Z is nearly equal to the number of electrons, the repulsive force between electrons and nucleus electrostatic attraction becomes larger, which means the electron correlation becomes important.

Four transitions for Li-like Cl calculated by Safronova and Safronova [30] were listed in Table III. Their results are only about 0.0007 Å higher than ours. Compared to experimental results, the maximum between ours and experimental results is 0.0032 Å. We think the present calculation is reliable, because of the experimental uncertainty (0.005 Å). The experimental transitions for $(^3S)^2P-{}^2S_{1/2}$ and $(^1S)^2P-{}^2S_{1/2}$ were blended [29], which need to be checked in future experiments.

Based on the model above, the K_α X-ray wavelengths, transition probability, line strengths in length gauge, and the ratios of velocity to length rates (A_v/A_l) from He-like chlorine through Ne-like chlorine are listed in Table IV. Though it is not possible to assess the accuracy of the complete set of data reported in this work, the good agreement between our values (listed in Table III) for He-like and Li-like chlorine and earlier theoretical [30] and experimental data [28, 29] can be taken as a measure of accuracy of our calculations.

4. Conclusion

Motivated by the need for accurate transition data in a variety of scientific applications, the EOL version of MCDF method is used to calculate the transition wavelengths, absorption oscillator strengths, and transition probability of the K_α X-ray from Cl(VIII) through Cl(XVI). At the same time, we can find that the length value is more stable in that it changes less as the active space extending. In this paper we give accurate transition properties from Cl(VIII) through Cl(XVI). These data provide reference value for level lifetime, charge state distribution, and average charge of chlorine plasma.

Acknowledgments

The authors are grateful to Vanderbilt University for providing the GRASPVU for free. This work is supported in part by the National Natural Science Foundation of China (grant No. 11174213 and 11304266).

References

[1] K.A. Berrington, S. Nakazaki, *At. Data Nucl. Data Tables* **82**, 1 (2002).

[2] N.C. Deb, D.S.F. Crothers, Z. Felifli, A.Z. Msezane, *J. Phys. B* **36**, L47 (2003).

[3] N. Singh, A.K.S. Jha, M. Mohan, *Eur. Phys. J. D* **38**, 285 (2006).

[4] P. Oliver, A. Hibbert, *J. Phys. B* **40**, 2847 (2007).

[5] P. Oliver, A. Hibbert, *J. Phys., Conf. Ser.* **130**, 012016 (2008).

[6] J.M. Bridges, W.L. Wiese, *Phys. Rev. A* **78**, 062508 (2008).

[7] S.S. Tayal, *Astron. Astrophys.* **426**, 717 (2004).

[8] R.M. Schectman, S.R. Federman, M. Brown, S. Cheng, M.C. Fritts, R.E. Irving, N.D. Gibson, *Astrophys. J.* **621**, 1159 (2005).

[9] A.M. Mossah, S.S. Tayal, *Astrophys. J. Suppl. Ser.* **202**, 12 (2012).

[10] A. Abou El-Maaref, M.A.M. Uosif, S.H. Allam, Th.M. El-Sherbini, *At. Data Nucl. Data Tables* **98**, 589 (2012).

[11] K.B. Choudhury, N.C. Deb, K. Roy, A.Z. Msezane, *Eur. Phys. J. D* **27**, 103 (2003).

[12] Neerja, G.P. Gupta, A.N. Tripathi, A.Z. Msezane, *At. Data Nucl. Data Tables* **84**, 85 (2003).

[13] P. Bogdanovich, R. Karpuškienė, I. Martinson, *Nucl. Instrum. Methods Phys. Res. B* **205**, 70 (2003).

[14] P. Bogdanovich, R. Karpuškienė, I. Martinson, *Phys. Scr.* **67**, 44 (2003).

[15] K.M. Aggarwal, F.P. Keenan, *At. Data Nucl. Data Tables* **99**, 156 (2013).

[16] A. Sengebusch, S.H. Glenzer, A.L. Kritcher, H. Reinholz, G. Öpke, *Contrib. Plasma Phys.* **47**, 309 (2007).

[17] K.G. Dyall, I.P. Grant, C.T. Johnson, F.A. Parpia, E.P. Plummer, *Comput. Phys. Commun.* **55**, 425 (1989).

[18] F.A. Parpia, C. Froese Fischer, I.P. Grant, *Comput. Phys. Commun.* **94**, 249 (1996).

[19] A. Stathopoulos, C. Froese Fischer, *Comput. Phys. Commun.* **79**, 268 (1994).

[20] J. Olsen, M.R. Godefroid, P.A. Jonsson, P.A. Malmquist, C. Froese Fischer, *Phys. Rev. E* **52**, 4499 (1995).

[21] F. Hu, J.M. Yang, C.K. Wang, L.F. Jing, S.B. Chen, G. Jiang, H. Liu, L.H. Hao, *Phys. Rev. A* **84**, 042506 (2011).

[22] Y.G. Mulye, L. Natarajan, *Phys. Scr.* **69**, 24 (2004).

[23] L. Natarajan, *J. Phys. B, At. Mol. Opt. Phys.* **35**, 3179 (2002).

[24] I.P. Grant, *J. Phys. B, At. Mol. Opt. Phys.* **7**, 1458 (1974).

[25] P. Marketos, *Z. Phys. D* **29**, 247 (1994).

[26] J.P. Santos, A.M. Costa, C. Madruga, F. Parente, P. Indelicato, *Eur. Phys. J. D* **63**, 89 (2011).

[27] P.H. Norrington, available at www.am.qub.ac.uk (2002).

[28] R.L. Kelly, *J. Phys. Chem. Ref. Data* **16**, supplement 1 (1987).

[29] V.A. Boiko, A.Ya. Faenov, S.A. Pikuz, *J. Quantum Spectrosc. Radiat. Trasnsfer* **19**, 11 (1978).

[30] U.I. Safronova, M.S. Safronova, *Mol. Phys.* **102**, 1331 (2007).